Macromolecules
ARTICLE

New Insights on the Strain-Induced Mesophase of Poly(D,L-lactide): *In Situ* WAXS and DSC Study of the Thermo-Mechanical Stability

G. Stoclet,*,† R. Seguela,*,† J.-M. Lefebvre,† and C. Rochas‡

†*Université de Lille Nord de France, UMR CNRS 8207, Unité Matériaux et Transformations, Université Lille1, Bâtiment C6, 59655 Villeneuve d'Ascq, France, and* ‡*Centre de Recherches sur les Macromolécules Végétales - CNRS - UPR 5301, BP 53, Domaine Universitaire de Saint Matin d'Hères, 38041 Grenoble, France*

ABSTRACT: This work deals with the study of the mesomorphic form or mesophase induced by tensile drawing from the amorphous state of a polylactide material containing 4 mol % of D-stereoisomer units. Investigations have been carried out over the draw temperature domain 45−90 °C, i.e. an interval spanning roughly ±20 °C about the glass transition temperature. *In situ* WAXS experiments during drawing, stress relaxation, and/or heating of stretched samples invariably showed the strain-induced occurrence of the mesophase as far as temperature did not exceed 70 °C. This seems to be the upper stability temperature of the mesophase identified in a previous study. DSC traces upon heating of drawn samples exhibit a post glass transition endothermic peak similar to the enthalpy relaxation phenomenon observed for aged polymers. The amplitude of this strain-induced endotherm proved to be strongly dependent on draw temperature and draw ratio. Draw ratio also appeared to strongly influence the temperature domain of cold crystallization. The quite different structural evolution of the drawn samples as a function of temperature, depending whether cold crystallization occurred close or far from the strain-induced endotherm, led us to the conclusion that this endotherm results from neither physical aging nor orientation relaxation but from "melting" of the mesophase. This proposal is thoroughly supported by the insensitivity of the endotherm enthalpy to the DSC scanning rate that gives evidence of a first order thermodynamic transition in contrast to the case of aging-induced endotherm. WAXS as a function of temperature on drawn samples annealed with free ends enabled to probe the persistence of chain orientation and the stability of the strain-induced structural changes in relation to drawing conditions.

Introduction

Poly(lactic acid) or polylactide (PLA) is a kind of biosourced polymer with promising capabilities for structural applications in substitution of oil-based plastics. However, as most of the presently known biopolymers, PLA cannot actually challenge the so-called commodity plastics in the domain of mechanical performances, noticeably regarding strength and resilience.[1,2] Compounding with fillers of high form factor and/or blending with more or less compatible polymeric compounds has been largely investigated for PLA mechanical reinforcement.[3−6] Alternatively, texturing via plastic deformation is well-known to improve stiffness and strength of semicrystalline polymers, particularly in the field of fibers and films, and barrier properties of films as well. This has opened new routes for optimizing PLA physical properties.[7−14]

In a former study[15] we investigated the tensile drawing behavior of a PLA material with 4.3% of D-isomer units. The structural characterization via *ex situ* X-ray measurements showed that strain-induced crystallization into the so-called disordered α-form occurred upon drawing at 90 °C, i.e., about 30 °C above the glass transition temperature, T_g. Drawing at $T_g + 10$ °C resulted in a structural ordering of the mesomorphic type. In the mid-temperature range, both crystal and mesophase were shown to coexist.

The mesophase was clearly identified via a well-defined WAXS reflection having constant values of both angular position and full-width at half-maximum (fwhm). The fwhm value ≈3.5° was an evidence of an intermediate ordering between the crystalline state (fwhm ≈0.5°) and the amorphous state (fwhm ≈8°). The thermodynamic stability of the mesophase was briefly discussed in terms of molecular mobility by means of dynamic mechanical analysis of the material in the temperature range of the main relaxation of the amorphous phase.

Mulligan and Cakmak previously reported on a nematic order in drawn PLA, without further comment.[10] In a more recent paper dealing with the phase transitions in quenched PLLA−PEG−PLLA block copolymers, Zhang et al.[16] reported the identification of a PLLA mesomorphic form by means of infrared spectroscopy. Besides, this mesophase was claimed to melt and recrystallize into the stable crystal form.

In the present paper, we report further insight into the strain-induced growth of PLA mesomorphic form via *in situ* WAXS experiments during stretching. Combined DSC and *ex situ* WAXS data also bring new information on the physical properties and thermo-mechanical stability of the mesophase.

Experimental Section

Material and Preparation. The polylactide (PLA) investigated in this work, containing 4.3 mol % of D-isomer units, was purchased from Natureworks (USA). The number-average and weight-average molar weights are M_n = 116 kDa and M_w = 188 kDa, respectively, according to the supplier. Pellets were compression-molded into 1 mm thick sheets between steel plates at 180 °C, and subsequently cooled down to room temperature (RT) at about 40 °C/min for preventing crystallization. Extrusion-blown films about 0.2 mm thick were also prepared according to a

*Corresponding authors. E-mail: (G.S.) gregory.stoclet@univ-lille1.fr; (R.S.) roland.seguela@univ-lille1.fr.

previously described procedure.[15] Sheets and films, both perfectly amorphous and isotropic, were systematically annealed for 15 min at 70 °C, i.e., $T_g + 10$ °C, and slowly cooled down to RT before every experiment in order to erase physical aging effects due to storage at RT.

Tensile Drawing. For the sake of *ex situ* structural studies of drawn samples, drawing experiments were carried out on an Instron tensile machine equipped with a temperature-regulated oven. The samples having 24 mm in gauge length and 5 mm in width were cut out from the blown films. The crosshead speed was 50 mm/min, i.e. an initial strain rate $\dot{\varepsilon} = 0.04$ s^{-1}. Parallel ink marks were printed along the sample in order to determine the local plastic strain, $\varepsilon = l/l_o$, where l and $l_o \approx 1.5$ mm are the intervals of the marks after and prior to drawing, respectively.

For the *in situ* WAXS study of the strain-induced structural changes, a homemade tensile testing stage allowing symmetrical drawing of the samples was used. Parallelepipedic test pieces 4 mm in gauge length and 3 mm wide were cut off the 1 mm thick sheets. The crosshead speed was 2.4 mm/min, i.e. an initial strain rate $\dot{\varepsilon} = 0.01$ s^{-1}. The nominal strain is defined as $\varepsilon_N = L/L_o$, where L and L_o are the gauge lengths of the sample during and prior to deformation, respectively. In some occasions, the nominal stress $\sigma_N = F/S_o$ was computed from the applied force, F, and the initial sample cross-section area, S_o.

Wide-Angle X-ray Scattering (WAXS). WAXS measurements were carried out on the BM02 beamline at the European Synchrotron Radiation Facility (Grenoble, France) equipped with a 0.5 mm point-focusing collimation, and using an X-ray energy of 24 keV (wavelength 0.51 Å). For the *in situ* drawing characterization, the through-view 2D-patterns were recorded using a CCD camera from Princeton Instruments, the acquisition time being 5 s every 7 s. Corrections were applied for background scattering, geometry and intensity distortions of the detector.

Both incoming and transmitted intensities were measured synchronously with WAXS data acquisition. Thereby the transmission factor, defined as the ratio between the transmitted intensity and the incident intensity, was calculated

Radial intensity profiles, $I(2\theta)$, were obtained by 180°-azimuth integrations of the 2D-patterns over 180° by means of the FIT2D software. Quantitative assessment of the weight fractions of the amorphous, mesomorphic and crystalline phases, X_{am}, X_{meso}, and X_{cr}, respectively, were made thanks to a previously described method[15] using the PeakFit software, and assuming Gaussian profiles for all scattering peaks and amorphous halo. Figure1 shows two examples of fitting azimuth-integrated WAXS profiles of samples drawn up to strain-hardening at $T_d = 70$ °C and $T_d = 80$ °C, from the former *ex situ* study.[15]

The amorphous intensity profile was experimentally identified regarding position and fwhm to the scattering pattern of the thoroughly amorphous sample. The strain-induced crystalline α′ form was clearly identified at $T_d > 80$ °C by sharp peaks having fixed angular position: only the fwhm and intensity were allowed to self-adjust during the PeakFit treatment of all WAXS profiles. Samples drawn just in glass transition temperature domain made it possible to identify the contribution of the mesomorphic form in the absence of crystal scattering.

Amorphous chain orientation was determined from sectorial analysis of the 2D-patterns using the main amorphous halo with scattering peak at $2\theta = 15°$. Consecutive 5°-sectors have been individually analyzed over a 180° azimuthal range using the above-described method in order to compute the $I(2\theta)$ radial intensity profiles for each phase as a function of the azimuth, ϕ, taken from the meridian. The azimuthal intensity profile, $I(\phi)$, of the amorphous phase was then computed for all drawn samples. The second moment of the orientation distribution function, i.e. the so-called Herman's orientation function of the amorphous phase,

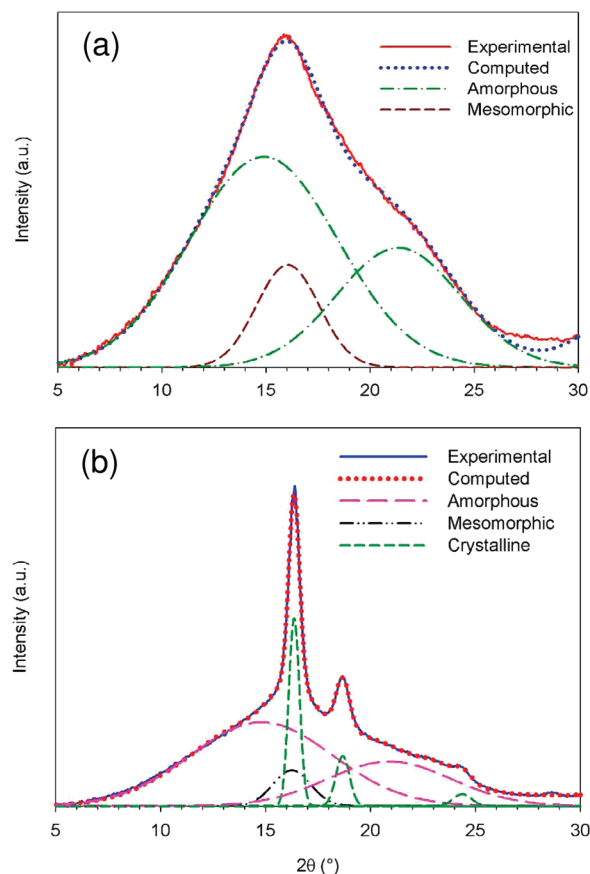$$P_2(\phi) = 3/2 \langle \cos^2 \phi \rangle - 1/2$$

Figure 1. Examples of PeakFit treatment of azimuth-integrated WAXS profiles of PLA samples drawn (a) at $T_d = 70$ °C to $\varepsilon \approx 360\%$ and (b) $T_d = 80$ °C to $\varepsilon \approx 360\%$ (data from the former *ex situ* study, see ref 15).

was computed as a function of draw ratio and draw temperature.

Differential Scanning Calorimetry (DSC). DSC measurements were performed on a Perkin-Elmer DSC7 apparatus. Temperature and heat flow scales were calibrated with high purity indium standard. Samples of about 6 mg were scanned under nitrogen gas flow at a heating rate of 10 °C/min, if not specified. In case of experiments involving various heating rates, calibration was carried out for each heating rate. Drawn samples were scanned immediately after drawing in order to prevent physical aging. In some cases, drawn samples were kept tightly clamped in the aluminum pans for preventing entropic shrinkage when heated above T_g. The clamping efficiency was checked *a posteriori* by opening the pan after the DSC heating scan. *Ex situ* WAXS measurements were performed on drawn samples in parallel to DSC analysis. The samples were heated in the DSC apparatus up to the desired temperature and immediately cooled down to RT before recording the so-called *ex situ* WAXS patterns.

Fourier Transform Infrared Spectroscopy (FTIR). FTIR spectra were collected in transmission mode on a Perkin-Elmer 2000 spectrometer equipped with a narrow range MCT detector, using 0.2 mm thick blown films. Unpolarized light was used to break free from orientation effects in the purpose of identification of the various phases. Every spectrum consisting of 130 scans with a resolution of 2 cm^{-1} was recorded over the wavenumber range 880−970 cm^{-1} according to Zhang et al.[16] The reduced absorbance was computed with respect to the sample thickness.

Dynamic Mechanical Thermal Analysis (DMTA). DMTA has been performed on an ARES equipment from TA Instruments using 1 mm thick parallelepipedic test pieces 30 mm in gauge

length and 12.5 mm wide. Storage and loss moduli, G' and G'' respectively, were determined from isochronal measurements over the temperature range 30−120 °C and the frequency range $10^{-2} - 10^2$ Hz, applying a shear strain of 0.1%. The Rouse relaxation time, τ_a, regarding the local motions between chain entanglements, was computed from the relation[17]

$$\tau_a = \frac{a^2 \xi (M_e/M_0)^2}{6\pi^2 kT} \quad (1)$$

where M_o is the molar mass of the monomer unit, M_e is the average molar mass of the chain segments between two consecutive entanglements, $a^2\xi$ is a so-called friction coefficient, and T is the temperature. M_e was computed according to the following relationship:

$$M_e = \frac{\rho RT}{G_N^0} \quad (eq2)$$

where the rubbery elastic modulus, $G°_N$, is conventionally taken as the G' value at the temperature of the $G''(T)$ minimum just above the main relaxation, and ρ is the polymer density. The temperature dependent factor $a^2\xi$ was computed from:

$$G' = G'' = \left(\frac{a\rho N}{4M_0}\right)\left[\frac{\xi kT}{3}\right]^{1/2} f^{1/2} \quad (eq3)$$

by plotting the $G'(f)$ and $G''(f)$ master curves for each temperature of investigation, the frequency f being taken at the intersection of the curves.

Results and discussion

***In situ* WAXS Analysis of PLA Drawing.** WAXS patterns recorded at various strains for $T_d = 45$ °C and $T_d = 75$ °C are reported in Figure 2. At first sight, these patterns are similar to the ones recorded in the *ex situ* study for equivalent draw conditions. If strain-induced chain orientation occurs for both temperatures, below and above T_g, one must note that crystalline spots only occur for $T_d = 75$ °C.

It was shown in the former *ex situ* WAXS study[15] that the mesomorphic phase already occurs when PLA is drawn far below its glass transition temperature, namely $T_d = T_g - 25$ °C. Figure 3 shows the *in situ* evolution of phase contents with nominal strain in amorphous PLA upon drawing at $T_d = 45$ °C $\approx T_g - 15$ °C. The sudden jump in the I/I_o plot gives indication of a plastic instability or necking involving a strong local strain heterogeneity along the sample. It turns out that the mesophase appears as soon as the neck shoulder enters the X-ray beam. Then the mesophase content gradually increases up to $X_{meso} \approx$ 10% as neck propagates. This is rather surprising since the local strain remains roughly constant in the necked region. If this finding confirms the capability of amorphous PLA to develop mesomorphic ordering at draw temperatures substantially below T_g, it also gives evidence that the kinetics of chain ordering are relatively slow. The slow chain ordering below T_g may have been activated by (1) slight creep during neck propagation and (2) self-heating that is generated in the neck shoulder.

However, considering both the small sample thickness and the low strain rate, one may expect a weak increase of local temperature, and definitely not exceeding T_g.

Regarding drawing at $T_d = 65$ °C $\approx T_g + 5$ °C, Figure 4 shows a roughly monotonic increase of I/I_o that reveals a fairly regular increase in the actual local strain upon increasing nominal strain. The mesomorphic phase appears first at $\varepsilon_N \approx 100\%$, then increases monotonically before leveling off at $X_{meso} \approx 10\%$ prior to rupture. The kinetics of chain
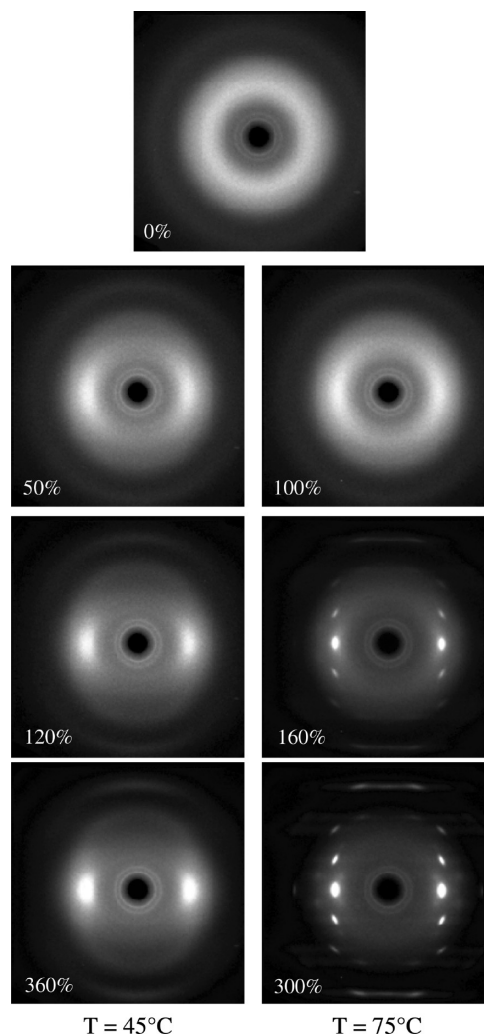

Figure 2. *In situ* WAXS patterns of PLA recorded at various strains during the drawing at temperatures $T_d = 45$ °C and $T_d = 75$ °C (the draw axis is vertical).
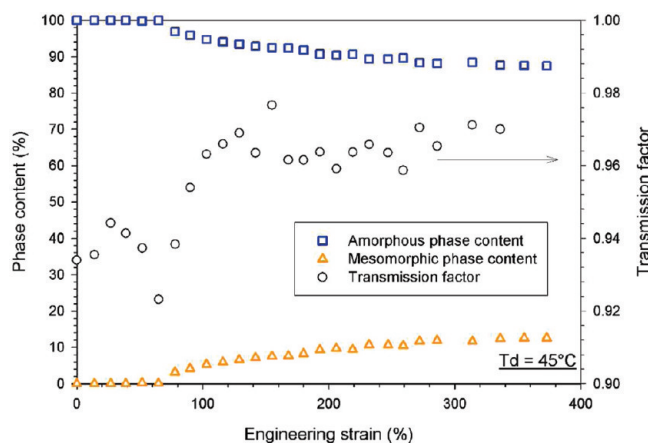

Figure 3. Evolution with nominal strain of the various phase contents computed from in situ WAXS in PLA upon drawing at $T_d = 45$ °C.

ordering turn out to be much faster than in the previous case $T_d = 45$ °C. Yet, no trace of crystalline order can be detected before reaching rupture. At this stage, one may not conclude whether strain-induced crystallization is governed by kinetics or thermodynamics, or both.

For drawing at $T_d = 70$ °C $\approx T_g + 10$ °C, the transmission factor data of Figure 5 give indication of a monotonic
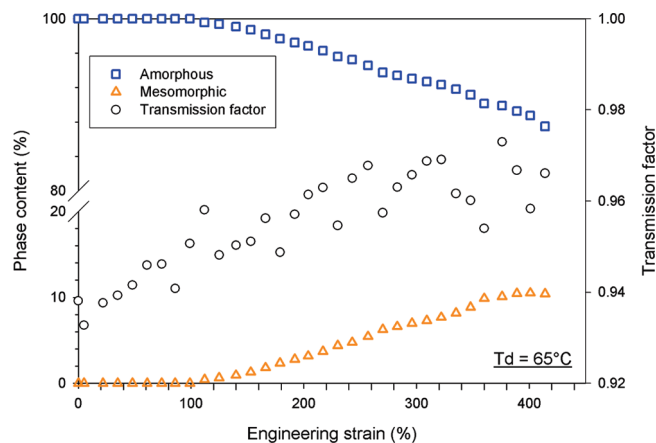
Figure 4. Evolution with nominal strain of the various phase contents computed from in situ WAXS in PLA upon drawing at $T_d = 65$ °C.

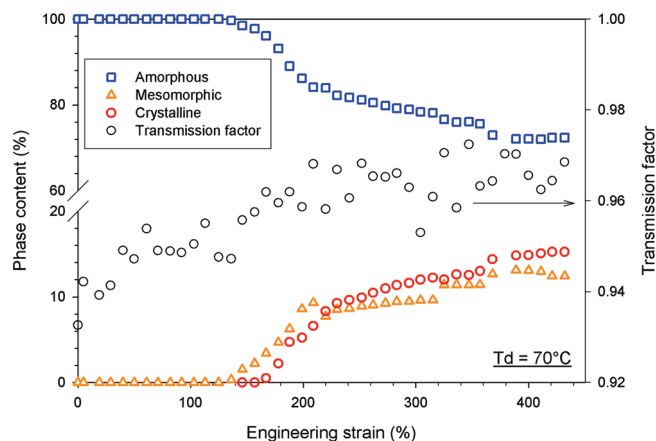**Figure 5.** Evolution with nominal strain of the various phase contents computed from in situ WAXS in PLA upon drawing at $T_d = 70$ °C.

Figure 6. Evolution with nominal strain of the various phase contents computed from in situ WAXS in PLA upon drawing at $T_d = 75$ °C.

Figure 7. Second moment $P_2(\phi)$ of the orientation distribution function of the amorphous phase versus nominal strain for draw temperatures 65 and 75 °C (for the sake of comparison $P_2(\phi)$ data have also been computed for samples drawn at $T_d = 90$ °C and $\dot{\varepsilon} = 0.04$ s^{-1} from the former study: see ref 15).

increase in the local strain, i.e., a roughly uniform deformation at a macroscopic scale. The mesophase formation onset appears at $\varepsilon_N \approx 140\%$, just before the occurrence of the crystalline α' phase. Both phase contents increase in parallel, up to rupture where $X_{meso} \approx 12\%$ and $X_{cr} \approx 15\%$. These data contrast with the former *ex situ* study that did not reveal any crystalline phase at the same draw temperature. This can be ascribed to the strain rate that is presently four times lower. It points out the incidence of kinetics on the mechanisms of strain-induced crystallization.

In Figure 6, are reported the data relevant to the drawing behavior at $T_d = 75$ °C. No trace of mesophase is detected for the duration of the *in situ* WAXS whereas the crystalline α' phase occurs at $\varepsilon_N \approx 150\%$. The sudden jump to $X_{cr} \approx 30\%$ is a strong indication of very fast ordering kinetics when sufficient orientation is reached. Besides, it is worth noticing that in the previous study carried out at higher strain rate, similar X_{cr} evolution was observed for $T_d = 90$ °C. This finding indicates that the occurrence of the mesophase requires that chain dynamics[15] are not too high in order to prevent molecular ordering into crystal.

The above findings are consistent with the conclusions from the previous *ex situ* study. Increasing the draw temperature involves a shift to higher value of the strain onset mesophase appearance. This points out the detrimental effect of chain relaxation on chain orientation that delays the buildup of chain ordering into mesophase. This is corroborated by the fact that, at equivalent temperature, the mesophase strain onset is somewhat higher in the present study carried out at a lower
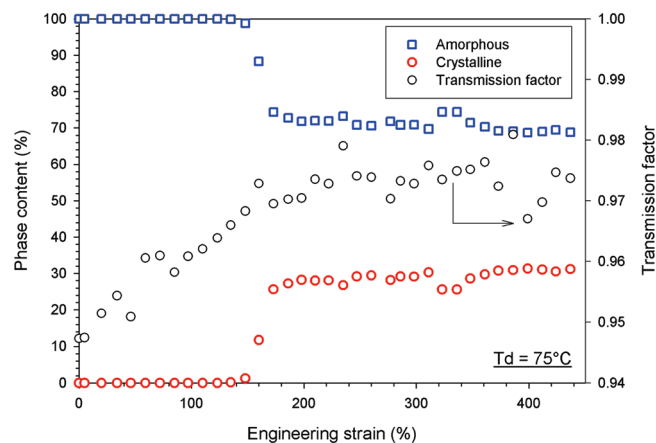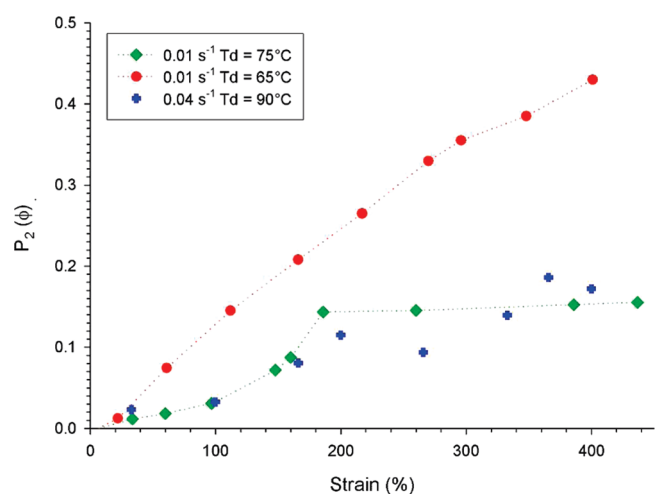
strain rate. As a matter of fact, the $P_2(\phi)$ data of Figure 7 show that an increase of draw temperature from 65 to 75 °C at $\dot{\varepsilon} = 0.01$ s^{-1} significantly reduces the orientation of the amorphous chains over the whole strain domain. Conversely, increasing the strain rate from 0.01 to 0.04 s^{-1} results in a similar level of chain orientation if the draw temperature is increased from 70 to 90 °C. It is however worth noticing that chain relaxation has a beneficial effect on the occurrence of the conformational rearrangements that are necessary for crystalline ordering. Indeed, stretching is more favorable to the chain-extended zigzag conformation than to the helical conformation characteristic of the α' crystal form. This is the reason why the upper temperature limit at which the strain-induced ordering turns from mesophase to crystal is slightly lower in the present study due to the lower strain rate.

Quantitative support to the above argumentation is given in Figure 8 that reports the computed relaxation times for amorphous PLA as a function of temperature. This approach borrows from Mahendrasingam et al.'s work regarding the strain-induced crystallization of poly(ethylene-terephthalate) in relation to chain mobility.[18,19] At strain rate $\dot{\varepsilon} = 0.01$ s^{-1} for the present study, only mesophase occurs at $T_d = 65$ °C since the relaxation rate $1/\tau_a < \dot{\varepsilon}$. At $T_d = 70$ °C, when the relaxation rate $1/\tau_a > \dot{\varepsilon}$, both mesophase and crystal are
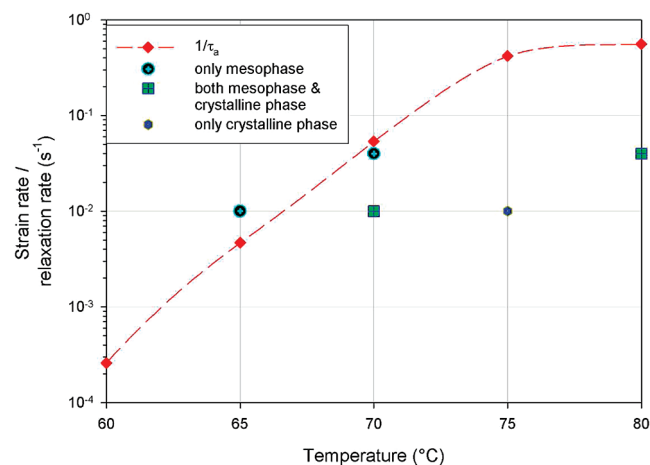
Figure 8. Rouse relaxation rate versus temperature for amorphous PLA (experimental data for the present and the former studies carried out at two different strain rates).
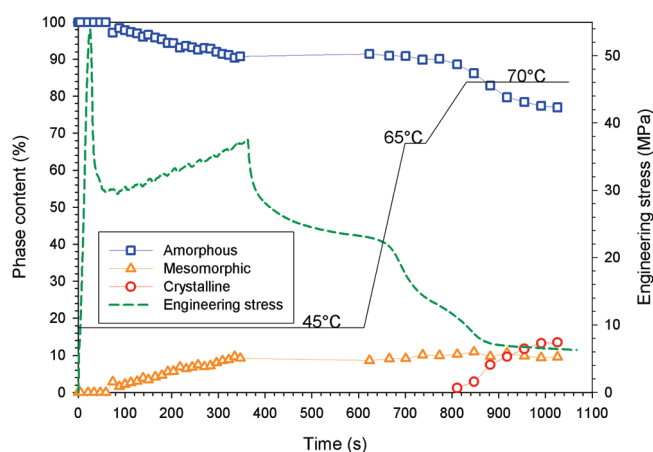

Figure 9. Time evolution of the various phase contents computed from in situ WAXS during relaxation after drawing PLA at $T_d = 45\,°C$, and further heating above 45 °C.

observed. At $T_d = 75\,°C$, only crystal is formed when the relaxation rate $1/\tau_a \gg \dot{\varepsilon}$. Also reported in Figure 8 are data from the former *ex situ* study carried out at the strain rate $\dot{\varepsilon} = 0.04\ s^{-1}$. These data show that the stability limit of the mesophase is slightly shifted to higher temperature as compared to the previous case, according to the $1/\tau_a$ dependence on temperature.

To sum up, chain relaxation must be restricted during drawing to enable mesomorphic ordering thanks to chain orientation. By contrast, some local relaxation motions are requested to promote crystalline order via conformational rearrangements.

Figure 9 reports the *in situ* evolution with time of the various phase contents in PLA during a multiple-sequence thermo-mechanical treatment, together with nominal stress and temperature. PLA is first drawn at $T_d = 45\,°C$.

The sharp yield point in the stress versus time plot is a strong hint to the occurrence of a plastic instability, as previously reported at the beginning of this subsection (Figure 3). The mesophase appears at time $t \approx 70\ s$ corresponding to neck stabilization, i.e., the drop of nominal stress to the stress plateau beyond the yield point. The monotonic increase of mesophase content up to $X_{meso} \approx 10\%$ is quite consistent with the previous data of Figure 3. Drawing is interrupted at $t = 360\ s$, i.e., just before break. PLA is then allowed to relax at constant strain until $t = 600\ s$, at
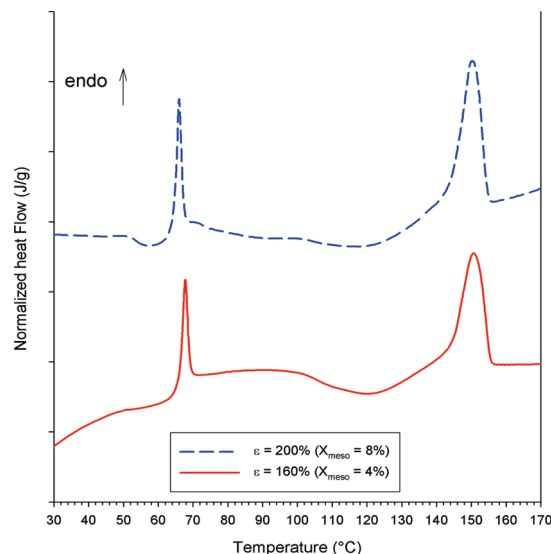

Figure 10. DSC traces of PLA samples drawn at $T_d = 45\,°C$ as a function of local strain (between brackets is indicated the mesophase content of each sample).

a roughly constant temperature of 45 °C. In the meantime, the mesophase content remains strictly constant. Temperature is then rapidly increased to 65 °C at time $t = 700\ s$, with no change in both X_{meso}, and X_a. Temperature is subsequently increased more slowly up to 70 °C at $t = 800\ s$. During this step, the crystalline phase gradually appears at the expense of the amorphous phase, the mesophase content remaining roughly constant.

This experiment has a double issue. First, it emphasizes the "dynamic" thermo-mechanical stability of the mesophase up to 70 °C at least, as previously concluded from the *ex situ* study on quenched samples. Second, it provides evidence that crystal growth from the oriented material requires that the temperature is increased above T_g to promote some chain mobility. X_{meso} invariance in parallel to X_{cr} increase during the isothermal treatment at 70 °C suggests that either 1) the crystalline phase directly grows from the oriented amorphous phase or 2) the mesophase grows from the oriented amorphous phase before acting as a precursor for crystal ordering. However the kinetics of the mesophase-crystal transition are low enough at 70 °C to enable a roughly constant amount of mesophase to be retained during the process. The next two subsections report attempts to solve this question.

Thermal Behavior of Drawn PLA. The thermal stability of the strain-induced structure of PLA has been investigated via DSC as a function of draw temperature and draw ratio. Figure 10 shows the DSC heating traces of two samples drawn at $T_d = 45\,°C$, a temperature far below T_g for which we formerly showed that the mesophase readily occurs upon drawing.[15] The strain $\varepsilon = 160\%$ relates to the neck, whereas the strain $\varepsilon = 200\%$ is prior to break. Four major phenomena are worth noticing in relation to increasing strain: (1) the appearance of an exotherm just before the glass transition; (2) an increasing endothermic peak just above the glass transition; (3) a broad exotherm shifting to low temperature; (4) an increasing high temperature endotherm.

First, the pre-T_g exotherm has been reported on some occasions regarding glassy polymers plastically deformed below T_g.[20−23] It has been assigned to the relaxation of plastic strain due to early activation of molecular mobility benefiting from the increase in free volume induced by plasticity defects.[24,25] The concomitant enthalpy increase

brought about by these defects is responsible for the exothermic effect during relaxation. Second, the sharp endotherm just above the glass transition is similar to the one associated with the aging-induced enthalpy relaxation of amorphous polymers resulting from thermodynamic stabilization, i.e. enthalpy decrease.[26−28] This phenomenon will be further addressed below in this subsection. Third, the broad exotherm spanning the range 75−140 °C is a hint of cold-crystallization promoted by the strain-induced orientation of the amorphous chains. The higher the draw ratio, the lower the peak temperature and the higher the amplitude of the exotherm. This underlines the crystallization kinetics improvement due to increasing chain orientation. Fourth, the high temperature endotherm located at about 160 °C results from the melting of the crystals grown from cold-crystallization. Its area gradually increases with strain, in parallel to the cold-crystallization exotherm.

As already reported in literature, PLA has very low crystallization kinetics in the isotropic state.[12] Strain-induced chain orientation drastically improves the crystallization capabilities in terms of both kinetics and crystal content.

Regarding drawing at $T_d = 70$ °C, one should first notice from the DSC traces of Figure 11 that the post-T_g exotherm is absent. Indeed, considering the "plasticity defects" theory discussed above, no enthalpy increase due to frozen "excess free volume" can be expected when PLA is drawn in the rubbery state. In contrast, the post-T_g endotherm is present. It is worth noticing that this endotherm turns out to be as much important as the melting endotherm at high strains, an observation never reported in the case of physical aging of semicrystalline polymers, to our knowledge. The cold-crystallization exotherm that appears in the range 90−140 °C grows with increasing strain up to $\varepsilon \approx 100\%$, as shown in the evolution of the crystallization enthalpy, ΔH_{cc}, reported in Figure 12. Beyond $\varepsilon \approx 100\%$, the crystallization exotherm shifts to the range 70−120 °C (Figure 11) while ΔH_{cc} levels off in the meantime (Figure 12). The temperature shift is an obvious consequence of increasing chain orientation that promotes earlier cold-crystallization. The concomitant ΔH_{cc} stabilization results from the occurrence of the strain-induced crystallization in parallel with the mesophase (Figure 5), so that less crystals can grow during the DSC heating scan. Regarding the melting endotherm, it is worth noticing the change from a double peak at low strain to a single sharp peak at large strains. In previous studies of isothermally crystallized polylactide, double melting peak has been assigned to either a melting/recrystallization of unstable crystals[29−32] or to the melting of a double population of crystals having different defect levels.[33−35] In the present case, a third likely issue is the occurrence of both α and α′ crystals during cold-crystallization, considering the very large breadth of the exotherm spanning on both sides of the critical temperature of 120 °C defined by Zhang et al.[36] Resolving this question would require further investigations that are out of the scope of this work focused on the mesomorphic form.

For drawing at $T_d = 80$ °C, Figure 13 exhibits roughly similar evolution with strain of the cold-crystallization exotherm and melting peak as in the case $T_d = 70$ °C. By contrast, the post-T_g endotherm is almost absent whatever the strain level. This striking difference from the two previous cases $T_d = 45$ °C and $T_d = 70$ °C, not reported so far in literature, is rather enigmatic and requires paying more attention to the phenomenon.

Numerous works regarding PLA and PLLA have reported the occurrence of the post-T_g endotherm as a result of aging as well as stretching below T_g.[31−45] Some authors
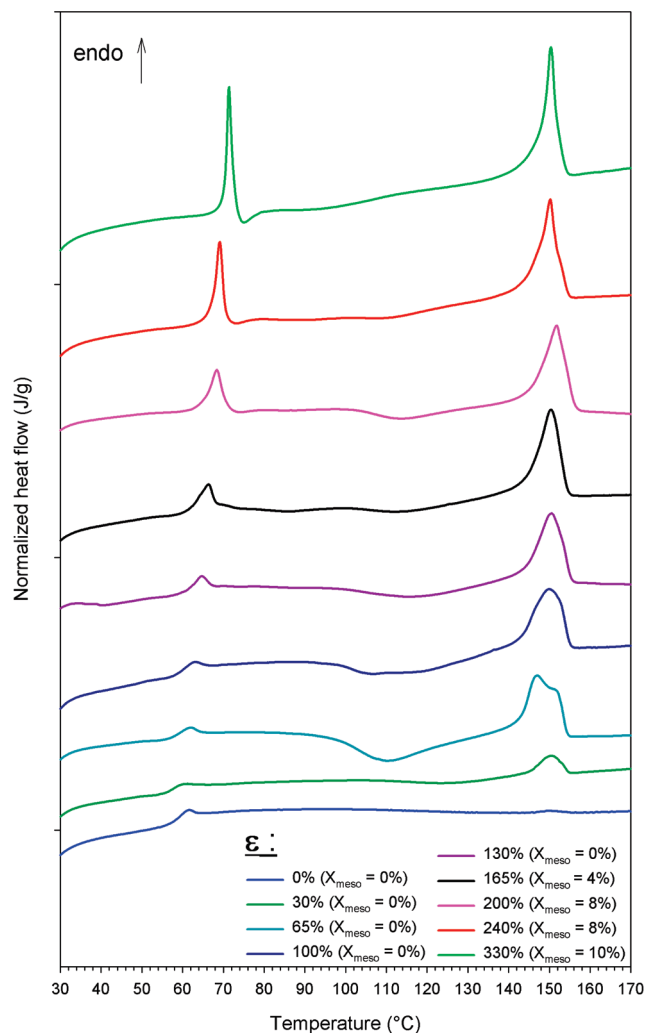
Figure 11. DSC traces of PLA samples drawn at $T_d = 70$ °C as a function of local strain (between brackets is indicated the mesophase content of each sample).
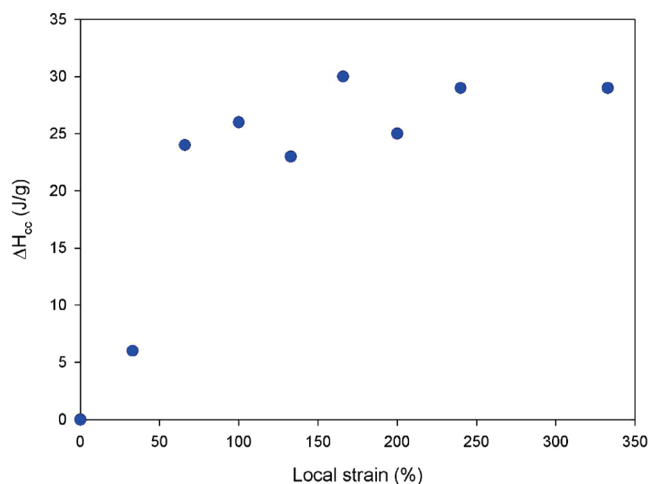
Figure 12. Cold-crystallization enthalpy versus local strain of PLA drawn at $T_d = 70$ °C.

claimed that the generation of local scale chain ordering in the amorphous state make it more stable via conformational rearrangements, in both circumstances.[42−45] Using Raman spectroscopy, Hsu and collaborators reported that conformational changes actually occur upon drawing[40,46] but not
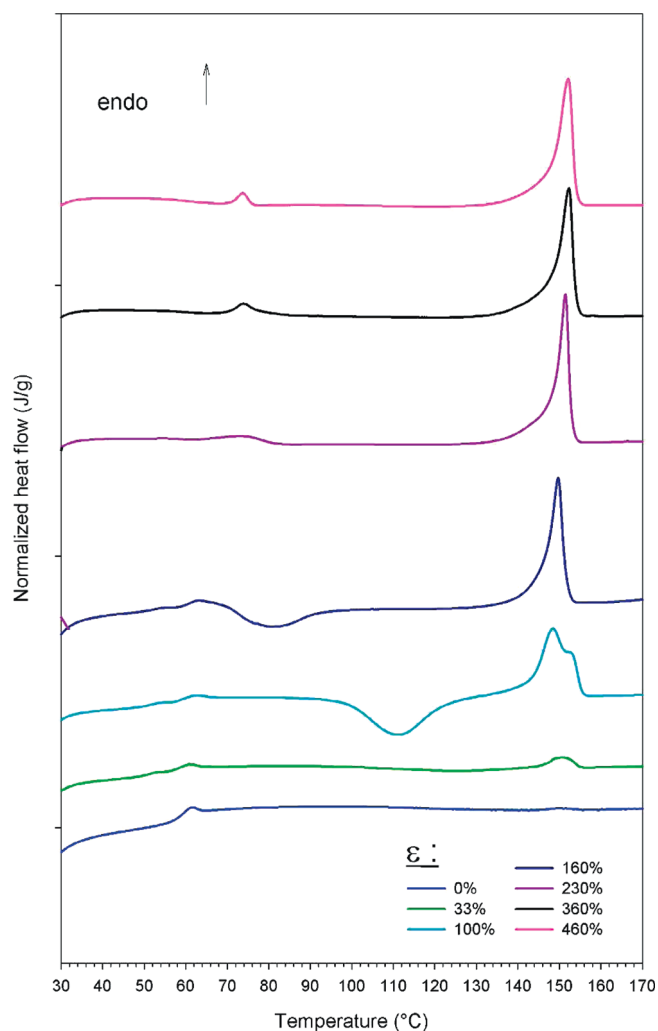
Figure 13. DSC traces of PLA samples drawn at $T_d = 80\ ^\circ\text{C}$ as a function of local strain.

appreciably upon aging.[41] In contrast, using Fourier-transform infrared spectroscopy (FTIR), Na et al.[45] claimed for observation of aging-induced growth of an ordered phase with dense intermolecular packing, as judged from slight conformational changes. These authors assigned the post-T_g enthalpy recovery to the melting of this ordered phase. The very recent work by Zhang et al.,[16] states identification of a mesophase in the PLLA domains of quenched PLLA−PEG−PLLA block copolymers by means of FTIR. Besides, this mesophase is clearly shown to melt and recrystallize into stable α crystals in the post-T_g temperature range. One may wonder whether the mesophases under concern in both the above study and the present one are similar or not. The FTIR spectra reported in Figure 14 for PLA samples drawn at $T_d = 70\ ^\circ\text{C}$ disclose a 918 cm^{-1} band that does not exist for either the amorphous or the crystalline phases and increases in parallel to the mesophase content, starting from $\varepsilon > 130\%$.

This band is precisely one of the specific bands assigned to the mesophase in Zhang et al.'s study. This is a strong hint that quench- and draw-induced mesophases in PLLA and PLA are identical from a conformational standpoint.

Regarding the present strain-induced post-T_g endotherm, specific features make us suspect that it originates from a phase transition associated with the presence of an ordered phase rather than from a common aging-induced enthalpy relaxation. Indeed, the post-T_g endotherm of drawn samples

can be almost as high and sharp as that of an aged sample. Clear evidence appears in Figure 15 by comparing the DSC trace of a sample aged for 3 years at RT with the DSC traces of drawn samples (Figures 10 and 11). For better comparison, one of these DSC traces has been reproduced in Figure 15 (PLA drawn to $\varepsilon = 200\%$ at $T_d = 70\ ^\circ\text{C}$).

This is all the more remarkable that drawn samples have been analyzed immediately after drawing, i.e., in the absence of any aging effect. Worth noticing is that various noncrystallizable polymers that display an enthalpy relaxation peak after aging below T_g do not exhibit the strong endotherm upon stretching.[20−23] This suggests that not only the strain-induced chain orientation is responsible for the post-T_g endotherm in PLA, but also that the capabilities of the polymer to build up an ordered structure are involved in the process. An alternative may thus be proposed considering the concomitant presence the strain-induced mesomorphic form according to WAXS. The fact that this phase no longer exists for $T_d > 70\ ^\circ\text{C}$, in parallel with the disappearance of the post-T_g endotherm (Figure 13), strongly suggests that 70 °C represents the upper limit of thermodynamic stability, otherwise the "melting" temperature of the mesophase. The next data aim at supporting this hypothesis.

Another major difference between the post-T_g endotherms of drawn and aged PLA lies in their kinetic behavior during the DSC scan. Figure 16 reports the endotherm enthalpy data versus heating rate for two PLA samples respectively drawn up to $\varepsilon \approx 160\%$ at $T_d = 45\ ^\circ\text{C}$ and to $\varepsilon \approx 200\%$ at $T_d = 70\ ^\circ\text{C}$. It is worth noticing that in both cases the crystallization exotherm does not interfere with the post-T_g endotherm so that it allows precise evaluation of the endotherm enthalpy (see Figures 10 and 11). For the sake of comparison, the data regarding PLA aged for about 3 years at RT in the isotropic state are also reported in Figure 16. The transition enthalpy for aged PLA is clearly heating rate dependent. This is an evidence for an enthalpy relaxation phenomenon associated with the glass transition that is a nonisothermal kinetic process. The phenomenon is sketched on the enthalpy versus temperature diagram of Figure 17 borrowed from Wunderlich:[21] following an aging treatment below T_g, the higher the DSC heating rate, the higher the enthalpy hysteresis due to deviation of the system from the liquid equilibrium line above T_g, and the greater the heat capacity overshoot. In contrast, the enthalpy invariance of the post-T_g endotherm for both drawn PLA samples (Figure 16) strongly suggests a first order transition, namely the melting of the mesophase.

Similar invariance of the post-T_g endotherm has been reported by Lee et al.[44] who concluded that it is a hint of conformational rearrangement from the oriented glass to the isotropic rubber state as a result of entropic shrinkage. The constant values of the endotherm enthalpy of about 3 and 5.5 J/g (Figure 16) for the two PLA samples drawn at the same strain but at different draw temperatures are of the order of magnitude of what may be expected for conformational changes in a thoroughly amorphous material, in agreement with Lee et al.'s conclusion. However, strain-induced chain orientation only is not sufficient to account for the occurrence of the strain-hardening in a noncrosslinked rubber (see Figure 3 in ref15), this phenomenon being usually ascribed to the growth of a cohesive phase. Alternatively, considering the strain-induced growth of the mesophase, and that $X_{meso} = 3−4\%$ for the sample drawn up to $\varepsilon = 160\%$ at $T_d = 45\ ^\circ\text{C}$ and $X_{meso} = 7−8\%$ for the sample drawn to up $\varepsilon = 200\%$ at $T_d = 70\ ^\circ\text{C}$, a specific melting enthalpy $\Delta H_m{}^{meso} \approx 70$ J/g can be estimated from the data

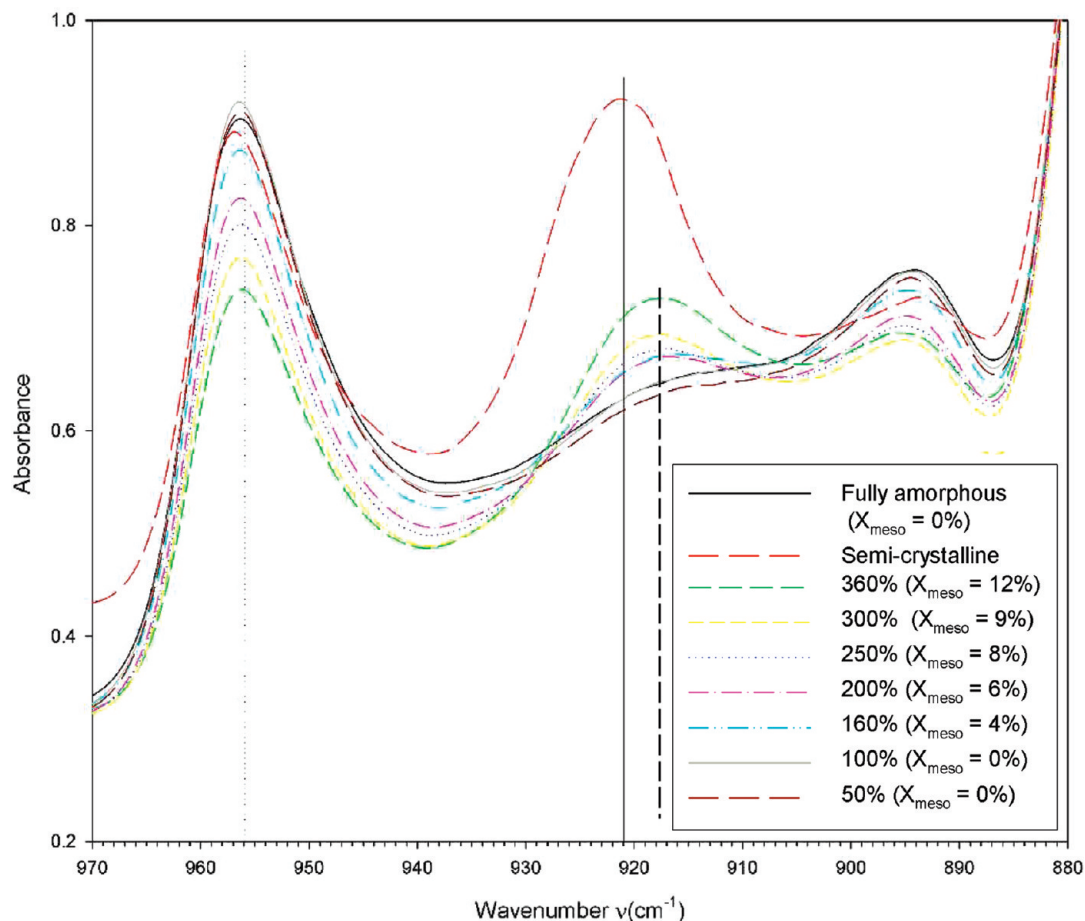**Figure 14.** Unpolarized FTIR spectra of PLA samples drawn at $T_d = 70\ ^\circ C$ as a function of local strain (in parentheses is indicated the mesophase content of every sample).
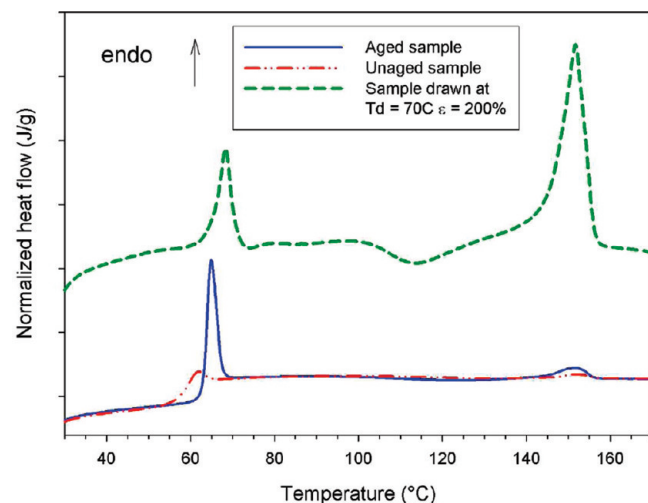

Figure 15. DSC traces of an isotropic amorphous PLA sample prior and after aging for about 3 years at room temperature (for the sake of comparison the DSC trace of PLA drawn to $\varepsilon = 200\%$ at $T_d = 70\ ^\circ C$).
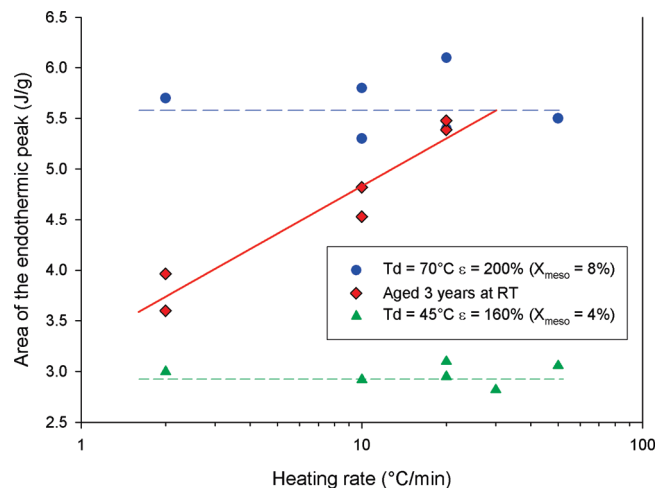

Figure 16. Variation with heating rate of the DSC post-T_g endotherm of PLA: (a) isotropic aged for about 3 years at room temperature; (b) drawn to $\varepsilon \approx 160\%$ at $T_d = 45\ ^\circ C$; (c) drawn to $\varepsilon \approx 200\%$ at $T_d = 70\ ^\circ C$ (between brackets is indicated the mesophase content of the drawn samples).

$\Delta H_{endo} \approx 3$ J/g and $\Delta H_{endo} \approx 5.5$ J/g for these two samples, respectively (Figure 16). Compared to the melting enthalpy $\Delta H_m^\circ \approx 95$ J/g of the PLA crystalline form,[39,47−49] the above ΔH_m^{meso} value gives clear evidence that the PLA mesophase is a highly cohesive state, in perfect agreement with the previous conclusions from the mechanical behavior.[15] More-over, this high ΔH_m^{meso} value indicates that the post-T_g endotherm arises from change in intermolecular interactions

rather than from conformational changes only, i.e. from a first order transition, as also concluded by Zhang et al.[16]

Benefiting from the above determination of ΔH_m^{meso}, the mesophase melting point can be assessed from the thermo-dynamic relation $T_m = \Delta H_m / \Delta S_m$, considering $\Delta H_m^\circ \approx 95$ J/g and $T_m^\circ \approx 150\ ^\circ C$ for the crystalline form, and assuming in first approximation that the melting entropy of the
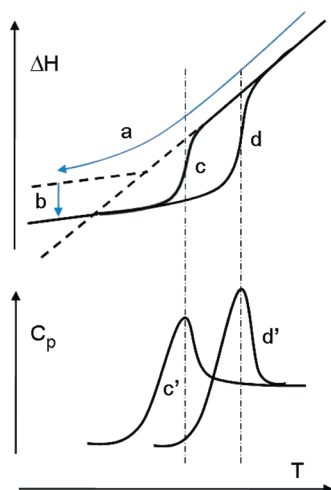
Figure 17. Schematic of the enthalpy and heat capacity variations with temperature in the domain of the glass transition of amorphous polymers: (a) slow cooling; (b) aging; (c) slow heating; (d) fast heating.

mesophase is 10% lower than that of the crystal due to the relative disorder of the former one. The estimated value $T_m^{meso} \approx 75$ °C turns out in very fair agreement with the temperature of the post-T_g endotherm.

Structural Changes upon Heating of Drawn PLA Samples. In order to progress in the evaluation of the thermo-mechanical stability of the mesophase, *ex situ* WAXS experiments have been carried out in parallel with DSC heating scans on drawn samples, for different draw temperatures and draw ratios.

Figure 18 and Figure 19 report the DSC traces and the associated WAXS patterns as a function of temperature for PLA samples drawn at $T_d = 70$ °C, the strain being $\varepsilon \approx 160\%$ and $\varepsilon \approx 360\%$ respectively in the two cases. Two major differences in the DSC traces are worth noticing: (1) the post-T_g endotherm is much more intense in the first case and (2) the cold-crystallization exotherm is shifted far beyond this endotherm. For $\varepsilon \approx 160\%$, the WAXS patterns show that the initially mesomorphic material turns amorphous during the glass transition process and shrinks back to the isotropic state. With increasing temperature, first signs of crystallization appear at the onset of the exotherm . Finally, sharp scattering rings can be seen at the end of the exotherm. In the case $\varepsilon \approx 360\%$, the WAXS patterns show that the initially mesomorphic material exhibits some crystalline reflections as soon as temperature reaches the temperature onset of glass transition. Surprisingly, no disorientation can be noted after completion of the glass transition. The crystalline spots are reinforced at the end of the post-T_g endotherm that coincides with the bottom of the cold-crystallization exotherm at about 75 °C. The broadness of the main equatorial spots yet strongly suggests that the oriented mesomorphic form is still present. Upon further temperature increase, i.e., about 110 °C, the crystalline reflections become sharper, including the main equatorial one.

Worth noticing is that the occurrence of the intense post-T_g endotherm for $\varepsilon \approx 160\%$ is concomitant with the shift of the exotherm to higher temperature. In the assumption of a cohesive mesophase, this could be associated with a complete melting of the mesophase beyond 70 °C (Figure 18) and the resulting chain randomization prior to crystallization in the liquid state. By contrast, for $\varepsilon \approx 360\%$, the shorter gap between the endotherm and the cold-crystallization exotherm, together with the observation that chain orientation is preserved in the temperature range 65–80 °C (Figure 19) suggest that a large part of the mesophase directly turns into
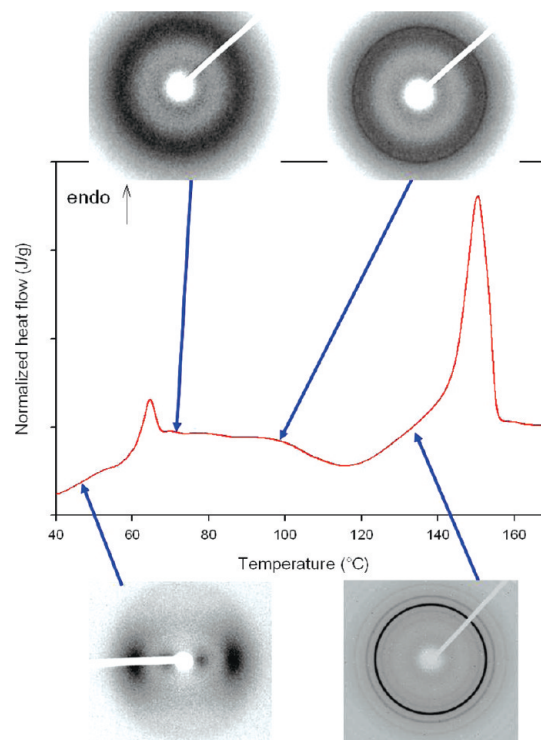

Figure 18. DSC trace and associated WAXS patterns as a function of temperature of a PLA sample drawn to $\varepsilon \approx 160\%$ at $T_d = 70$ °C (the draw axis is vertical).

Figure 19. DSC trace and associated WAXS patterns as a function of temperature of a PLA sample drawn to $\varepsilon \approx 360\%$ at $T_d = 70$ °C (the draw axis is vertical).
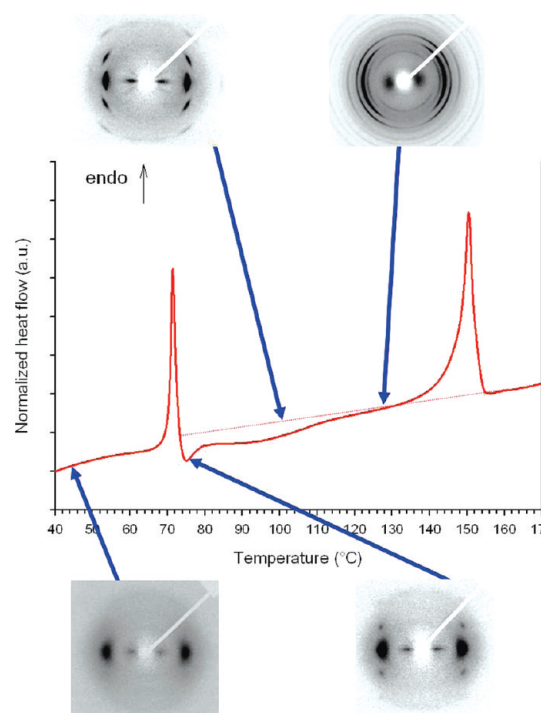
crystal in this temperature window without melting. Then crystal perfectness increases during further heating up to 120 °C. The small post-T_g endotherm may be assigned to the "melting" of only a part of the mesophase having lower cohesion than the average.

These present data unfortunately do not allow us to conclude whether the mesophase is actually precursory of

the crystalline form or not. Work is currently in progress in this aim.

Concluding Remarks

In the present work, special attention has been given to the characterization of the thermo-mechanical stability of the strain-induced mesomorphic order already evidenced in a former study of the tensile drawing of PLA above T_g. On the basis of *in situ* X-ray scattering data acquisition during drawing, this mesophase is shown to be thermodynamically stable over a short temperature range above T_g. For draw temperatures $T_d > 70\,°C$, only the α' crystalline phase is observed. The occurrences of a sharp post-T_g endotherm only for drawn PLA samples containing meso-phase provide evidence of the melting of the latter. These conclusions are thoroughly in line with recent spectroscopic studies giving convincing clues of the buildup of conformational ordering in drawn PLLA. If the growth of the mesophase involves kinetic factors governed by chain dynamics, as reflected in the dual incidence of temperature and strain rate, the mesophase melting exhibits the characteristic features of a first order thermodynamic transition. This finding excludes the eventuality of microcrystals previously proposed as an alternative to the mesophase.

The occurrence of the cold-crystallization upon heating beyond T_g may significantly affect the melting behavior of the mesophase, depending on the drawing conditions. Indeed, for high draw ratios, the occurrence of the cold-crystallization onset just after T_g entails an interference with the melting of the mesophase. In this case, a part of the mesophase does not actually melt but rather acts as a precursor to the crystalline phase during the DSC heating scan. For low draw ratios, the cold-crystallization onset is shifted far beyond T_g so that the mesophase is able to melt and disorient prior to crystallization, if the sample is kept unconstrained to allow thermal shrinkage.

The strain-induced mesophase of PLA is similar to the one already observed in PET and PEN.[50] In both polymers, the stacking of the planar aromatic rings is suspected to contribute to the mesomorphic ordering.[51−56] However, such rigid planar groups do not exist in PLA, so the question remains regarding the physical origin of the PLA mesophase. However, a major physical characteristic of the PLA mesophase is its cohesiveness almost as high as that of the crystal, quite similar to the case of PET mesophase.[57]

References and Notes

(1) Sinclair, R. G. *J. Macromol. Sci.—Pure Appl. Chem.* **1996**, *33*, 585–597.
(2) Auras, R. A.; Harte, B.; Selke, S. *Macromol. Biosci.* **2004**, *4*, 835–864.
(3) Bordes, P.; Pollet, E.; Averous, L. *Prog. Polym. Sci.* **2009**, *34*, 125–155.
(4) *Biodegradable Polymer Blends and Composites from Renewable Resources*; Yu, L., Ed.; John Wiley & Sons Inc.: Hoboken NJ; 2009.
(5) Ljungberg, N.; Wesslen, B. *Biomacromolecules* **2005**, *6*, 1789–1796.
(6) Schwach, E.; Six, J.-L.; Averous, L. *J. Polym. Environ.* **2008**, *16*, 286–297.
(7) Gupta, B.; Revagade, N.; Hilborn, J. *Prog. Polym. Sci.* **2007**, *32*, 455–482.
(8) Lima, L.-T.; Auras, R.; Rubino, M. *Prog. Polym. Sci.* **2008**, *33*, 820–852.
(9) Kumar, S.; Akhtar, S.; Kumar, V. *Pop. Plast. Packag.* **2005**, *50*, 85–89.
(10) Mulligan, J.; Cakmak, M. *Macromolecules* **2005**, *38*, 2333–2344.
(11) Ghosh, S.; Vasanthan, N. *J. Appl. Polym. Sci.* **2006**, *101*, 1210–1216.
(12) Stoclet, G.; Elkoun, S.; Miri, V.; Seguela, R.; Lefebvre, J. M. *Int. Polym. Process.* **2007**, *22*, 385–388.
(13) Pluta, M.; Galeski, A. *Biomacromolecules* **2007**, *8*, 1836–1843.
(14) Ou, X.; Cakmak, M. *Polymer* **2008**, *49*, 5344–5352.
(15) Stoclet, G.; Seguela, R.; Lefebvre, J.-M.; Elkoun, S.; Vanmansart, C. *Macromolecules* **2010**, *43*, 1488–1498.
(16) Zhang, J.; Duan, Y.; Domb, A. J.; Ozaki, Y. *Macromolecules* **2010**, *43*, 4240–4246.
(17) Doi, M.; Edwards, S. F. *The Theory of Polymer Dynamics*; Clarendon Press: Oxford, U.K., 1986.
(18) Blundell, D. J.; Mahendrasingam, A.; Martin, C.; Fuller, W.; MacKerron, D. H.; Harvie, J. L.; Oldman, R. J. *Polymer* **2000**, *41*, 7793–7802.
(19) Mahendrasingam, A.; Blundell, D. J.; Martin, C.; Fullerd, W.; MacKerron, D. H.; Harvie, J. L.; Oldman, R. J. *Polymer* **2000**, *41*, 7803–7814.
(20) Park, J. B.; Uhlmann, D. R. *J. Appl. Phys.* **1973**, *44*, 201–206.
(21) Wunderlich, B. *Macromolecular Physics, Vol. 2: Crystal Nucleation, Growth, Annealing*; Academic Press: New York; 1976; Chapter 7.
(22) Hasan, O. A.; Boyce, M. C. *Polymer* **1993**, *34*, 5085–5092.
(23) Quinson, R.; David, L.; Gauthier, C.; Perez, J. *Polym. Eng. Sci.* **1997**, *37*, 1633–1664.
(24) Oleinik, E. *Prog. Colloid Polym. Sci.* **1989**, *80*, 140–150.
(25) Munch, E.; Pelletier, J. M.; Sixou, B.; Vigier, G. *Phys. Rev. Lett.* **2006**, *97*, 207801/1–207801/4.
(26) Hutchinson, J. M. *Prog. Polym. Sci.* **1995**, *20*, 703–760.
(27) Faivre, A.; David, L.; Vassoille, R.; Vigier, G.; Etienne, S.; Geissler, E . *Macromolecules* **1996**, *29*, 8387–8390.
(28) Abbes, K.; Vigier, G.; Cavaille, J.-Y.; David, L.; Faivre, A.; Perez, J. *J. Non-Cryst. Solids* **1998**, *235−237*, 286–292.
(29) Sarasua, J.-R.; Prud'homme, R. E.; Wisniewski, M.; Le Borgne, A.; Spassky, N. *Macromolecules* **1998**, *31*, 3895–3905.
(30) Yasuniwa, M.; Tsubakihara, S.; Sugimoto, Y.; Nakafuku, C. *J. Polym. Sci., Polym. Phys.* **2004**, *42*, 25–32.
(31) Kulinski, Z.; Piorkowska, E. *Polymer* **2005**, *46*, 10290–10300.
(32) Solarski, S.; Ferreira, M.; Devaux, E. *Polym. Commun.* **2005**, *46*, 11187–11192.
(33) Pluta, M.; Galeski, A. *J. Appl. Polym. Sci.* **2002**, *86*, 1386–1395.
(34) Kim, M. S.; Kim, J. C.; Kim, Y. H. *Polym. Adv. Technol.* **2008**, *19*, 748–755.
(35) Magon, A.; Pyda, M. *Polymer* **2009**, *50*, 3967–3973.
(36) Zhang, J.; Tashiro, K.; Tsuji, H.; Domb, A. J. *Macromolecules* **2008**, *41*, 1352–1357.
(37) Lee, J. K.; Lee, K. H.; Jin, B. S. *Eur. Polym. J.* **2001**, *37*, 907–914.
(38) Celli, A.; Scandola, M. *Polymer* **1992**, *33*, 2699–2703.
(39) Pyda, M.; Wunderlich, B. *Macromolecules* **2005**, *38*, 10472–10479.
(40) Aou, K.; Kang, S.; Hsu, S. L. *Macromolecules* **2005**, *38*, 7730–7735.
(41) Aou, K.; Hsu, S. L.; Kleiner, L. W.; Tang, F. *J. Phys. Chem.* **2007**, *111*, 12322–12327.
(42) Pan, P.; Zhu, B.; Inoue, Y. *Macromolecules* **2007**, *40*, 9664–9671.
(43) Pan, P.; Zhu, B.; Dong, T.; Yazawa, K.; Shimizu, T.; Tansho, M.; Inoue, Y. *J. Chem. Phys.* **2008**, *129*, 184902/1–184902/10.
(44) Lee, S. G.; Han, J. I.; Jeong, Y. G.; Kwon, M. *Macromolecules* **2010**, *43*, 25–28.
(45) Na, B.; Lv, R.; Zou, S.; Li, Z.; Tian, N. *Macromolecules* **2010**, *43*, 1702–1705.
(46) Yang, X.; Kang, S.; Yang, Y.; Aou, K.; Hsu, S. L. *Polymer* **2004**, *45*, 4241–4248.
(47) Fischer, E. W.; Sterzel, H. J.; Wegner, G. *Kolloid Z. Z. Polym.* **1973**, *21*, 980–990.
(48) Huang, J.; Lisowski, M. S.; Runt, J.; Hall, E. S.; Kean, R. T.; Buehler, N.; Lin, J. S. *Macromolecules* **1998**, *31*, 2593–2599.
(49) Pyda, M.; Bopp, R. C.; Wunderlich, B. *J. Chem. Thermodyn.* **2004**, *36*, 731–742.
(50) Seguela, R. *J. Macromol. Sci., Polym. Rev.* **2005**, *45*, 263–287.
(51) Sun, T.; Zhang, A.; Li, F. M.; Porter, R. S. *Polymer* **1988**, *29*, 2115–2120.
(52) Welsh, G. E.; Blundell, D. J.; Windle, A. H. *J. Mater. Sci.* **2000**, *35*, 5225–5240.
(53) Ran, S.; Wang, Z.; Burger, C.; Chu, B.; Hsiao, B. S. *Macromolecules* **2002**, *35*, 10102–10107.
(54) Mahendrasingam, A.; Blundell, D. J.; Martin, C.; Urban, V.; Narayanan, T.; Fuller, W. *Polymer* **2005**, *46*, 6044–6049.
(55) Kawakami, D.; Hsiao, B. S.; Burger, C.; Ran, S.; Avila-Orta, C.; Sics, I.; Kikutani, T.; Jacob, K. I.; Chu, B. *Macromolecules* **2005**, *38*, 91–103.
(56) Abou-Kandil, A. I.; Goldbeck-Wood, G.; Windle, A. H. *Macromolecules* **2007**, *40*, 6448–6453.
(57) Abou-Kandil, A. I.; Flores, A.; Balta Calleja, F.-J.; Windle, A. H. *J. Polym. Res.* **2008**, *15*, 373–379.